Electronic Supplementary Information

Selective electro-reforming of waste polyethylene-terephthalate-derived ethylene glycol to C_2 chemicals with long-term stability

Yuxiang Wang, [a,b] Kesheng Liu, [a,b] Fulai Liu, [a] Chuxuan Liu,[a,b] Rui Shi,*[a] and Yong Chen*[a,b]

[a] *Key Laboratory of Photochemical Conversion and Optoelectronic Materials & CAS-HKU Joint Laboratory on New Materials, Technical Institute of Physics and Chemistry, Chinese Academy of Sciences, Beijing 100190, People's Republic of China. E-mail: shirui@mail.ipc.ac.cn, chenyong@mail.ipc.ac.cn*

[b] *University of Chinese Academy of Sciences, Beijing 100049, People's Republic of China*

Materials

All materials were of analytical grade and used as received without further purification. Graphite powder and Nafion perfluorinated resin solution were obtained from Alfa Aesar. Palladium chloride ($PdCl_2$), Chloroplatinic acid (H_2PtCl_6), hydrochloric acid (HCl), potassium hydroxide (KOH), polyethylene terephthalate (PET), glyoxal, ethylene glycol (EG), and D_2O were obtained from Sinopharm Chemcial Reagent Co., Ltd (Shanghai, China). Silver nitrate ($AgNO_3$), Sodium hypophosphite (NaH_2PO_2), $NaBH_4$, and N-Hexadecyltrimethylammonium Chloride (CTAC) were obtained from Alab (Shanghai) Chemical Technology Co., Ltd. Platinum foil was bought from Tianjin AIDA Hengsheng Science-Technology Development Co., Ltd. Commercial Pd /C was purchased from Energy Chemical. Deionized water was used in experiments and all reagents were used as received without further purification. Nafion N117 PEM was obtained from SCI Materials Hub.

Synthesis of the Pd_xAg_y NPs

In a typical synthesis, 6 ml of 0.05 M H_2PdCl_4 and 6 ml of 0.05 M $AgNO_3$ were added to 500 ml of 0.01 M CTAC aqueous solution under magnetic stirring for 10 min and ultrasonic for 10 min at room temperature. Then the solution was added dropwise with 10 ml of 0.2 M $NaBH_4$ in 5 min under magnetic stirring and kept at 25 ℃ for 1h. The solution containing black solid products was collected by precipitation and redispersed in deionized water. Repeat twice. The solution was quickly frozen using liquid N_2 and immediately transferred to a lyophilizer for lyophilization overnight. Other alloys with different compositions could be ach-ieved by adjusting the Pd/Ag precursor ratio.

The synthesis of the sample using ascorbic acid is unchanged except that $NaBH_4$ is replaced by ascorbic acid.

Synthesis of the Pt/NF

Nickle foam was first cleaned by acetone, ethanol and hydrochloric acid solution. H_2PtCl_6 was dissolved in 70 ml H_2O, and then transferred into a 100 ml Teflon-lined stainless steel autoclave. A piece of cleaned NF (2 × 3 cm^2) was immersed into the solution and placed against the wall of autoclave. Next the autoclave was maintained at 40℃ for 6h. The final product was washed several times using an ethanol solution after they were naturally cooled to room temperature. Finally, the as-prepared Pt/NF was dried in an oven at 60°C.

Synthesis of the Ni_2P/NF

Nickle foam was first cleaned by acetone, ethanol and hydrochloric acid solution. Then, the cleaned NF was placed in a vacuum oven dried at 65 °C for 8 h. The preprocessed NF and a certain amount of NaH_2PO_2 were put into a small porcelain boat. The air was first expelled by the Ar gas for 60 min with a flow rate at 50 ml min−1 . Subsequently, the samples were heated at 350 °C for 120 min at a heating rate of 3 °C min^{-1}. After cooling to the room temperature, where the Ar flowing was maintained throughout the overall process, the as-synthesized Ni_2P nanosheets were obtained and the color of the NF framework was changed to gray black.

Real-world plastic bottle pretreatment.

20 g real-world plastic bottle was pretreated in 100 mL of 10 M KOH solution at 80 °C

for 24 h, and the resulting suspension was used as electro-reforming substrate in a two-electrode system.

Materials characterization

X-ray diffraction (XRD) spectra were recorded on a Bruker D8 Focus diffractometer using Cu Kα (λ=1.5405 Å). The XRD data for indexing and cell-parameter calculation were collected in a scanning mode with a step length of 0.1° and a preset time of 1s/step. Chemical characterization of the sample surface was performed with X-ray photoelectron spectroscopy (XPS ThermoFisher ESCALAB 250Xi). The charge effect was calibrated using the binding energy of C1s. Morphologies of the as-prepared sample were characterized by Hitachi S-4800 field emission scanning electron microscope (SEM) and JEM 2100F transmission electron microscopy (TEM) operated at an accelerating voltage of 200 kV. Elemental analysis data of samples were obtained using inductively coupled plasma atomic emission spectrometry (ICP-OES Varian 710-OES, USA). The quantities of H_2 evolution were measured by a gas chromatograph (GC-2014C, Shimadzu, with Ar as carrier gas), which was equipped with a 5 Å molecular sieve column (3 m × 2 mm) and a thermal-conductivity detector.

Electrochemical measurements

A standard three-electrode system on CHI760E Electrochemical Work Station was used for electrochemical measurements. H-type cell separated by Nafion N117 PEM was used. A platinum foil, a glassy-carbon electrode (3mm in diameter), and a mercuric oxide electrode were used as the counter-, working-, and reference electrode, repectively. 2mg of PdAg NPs and 8mg graphite powder crystalline (as the conductive additive) were dispersed in 0.5ml deionized water and 1.5ml ethanol, added with 100 μl of 5wt% Nafion solution, and sonicated for 30min to form a uniform ink. Subsequently, 5μl of the catalyst ink was dropped onto the glassy carbon electrode to make the catalyst-coated working electrode and dried in air naturally. Electrocatalysts were first activated in 1 $_M$ KOH with CV method at a scan rate of 100mV s^{-1} for about 40 cycles. The electrocatalytic activity of Pd/NF for EG oxidation was investigated with CV method in KOH solution at a scan rate of 10 mV s^{-1}. EGOR tests were conducted in a 1 M KOH solution containing 1 M ethylene glycol. ECSA was estimated from the CV curve in 1 M KOH with Eq.1

$$ECSA = \frac{Q_{PdO}}{0.405\ mC\ cm^{-2} \times m_{pd}} \quad \text{Eq.1}$$

where Q_{PdO} was the charge by integrating the reduction peak area of PdO to Pd, m_{pd} was the Pd mass on the working electrode as determined by ICP, and $0.405\ mC\ cm^{-2}$ was the charge required for the reduction of PdO monolayer.

During the electro-reforming process, the concentrations of products were quantified by ^{1}H -NMR and ^{13}C-NMR spectroscopy. ^{1}H-NMR and ^{13}C-NMR spectroscopies were collected on a 700 MHz Bruker spectrometer. All NMR sample preparation is as follows: 300 μL product electrolyte + 300 μL D_2O + 30 μL DMSO (internal standard). The quantity of products in the samples was calculated by Eq.2

$$m_{product} = \frac{I_{Product} \times N_{DMSO} \times M_{product}}{I_{DMSO} \times N_{product} \times M_{DMSO}} \times m_{DMSO} \times n \quad \text{Eq. 2}$$

where $I_{product}$ is the integral of product peak; $N_{product}$ is the numbers of proton or carbon corresponding to product peak; $M_{product}$ is the molar mass of product; m_{DMSO} is the mass of DMSO; n = 60 mL/300 μL = 200.

The faradaic efficiency for EGOR was defined as the quantity of electric charges used for producing carbonate divided by the total charge passing through the electrodes during the electrolysis. Four electrons are needed to produce one glycolate ion, so the faradaic efficiency can be calculated by Eq. 3:

$$FE_{glycolate} = (4 \times m_{glycolate}/M_{glycolate} \times F)/Q \quad \text{Eq. 3}$$

where $m_{glycoltae}$ is the mass of potassium glycolate, $M_{glycolate}$ is molar mass of potassium glycolate, F is the faraday constant and Q is the total number of charges passing through the catalyst.

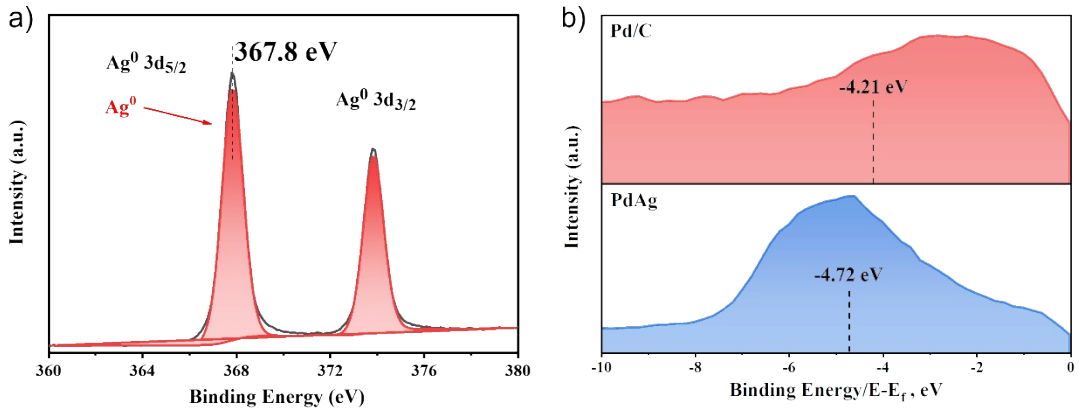

Fig. S1 (a) High-resolution Ag 3d XPS spectra of Pd-Ag NPs prepared with Ascorbic acid. (b)XPS valence band spectra of Pd/C and PdAg NPs. The calculated valance band centers are marked with dashed lines. The binding energy values were referenced using the C 1 s peak position at 284.8 eV. The XPS valance band centers were evaluated by applying the following formula.

$$valance\ band\ center = \int_{-10\ eV}^{0\ eV(E_f)} (binding\ energy(E) \times intensity(E))d\,E \Big/ \int_{-10\ eV}^{0\ eV(E_f)} intensity(E)d\,E$$

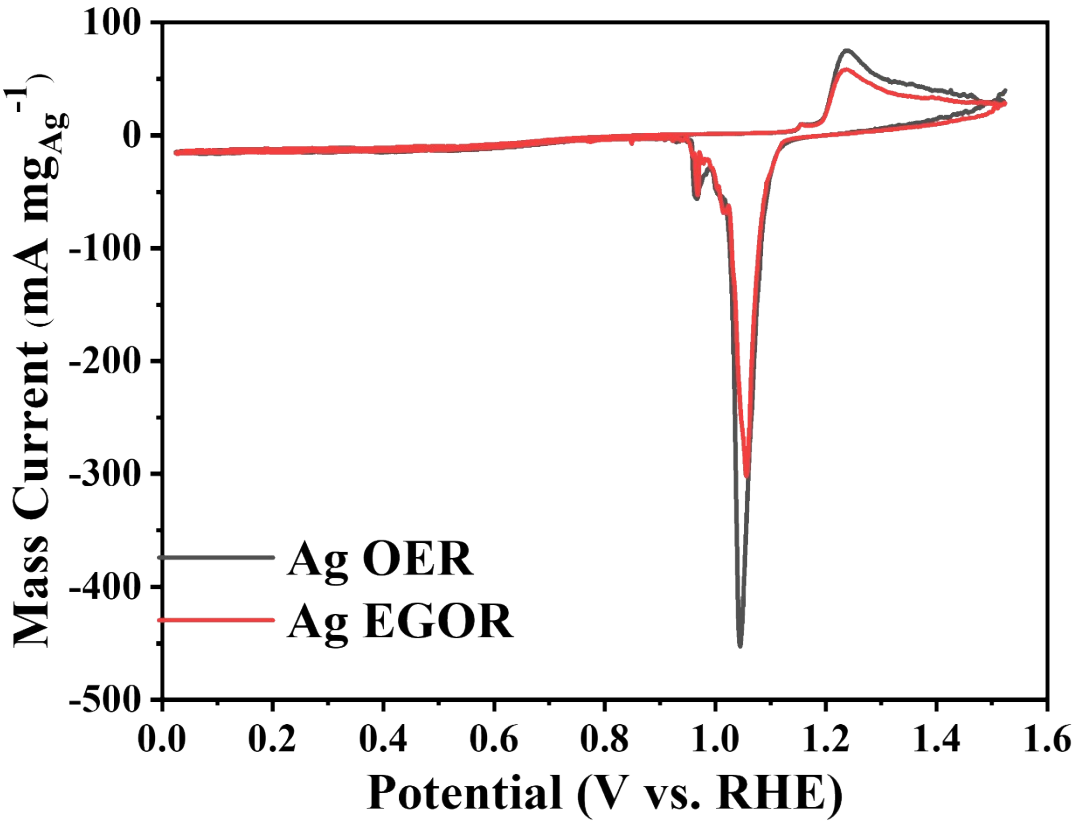

Fig. S2 CV curve of Ag NPs in 1 M KOH solution and 1 M KOH + 1 M EG solution.

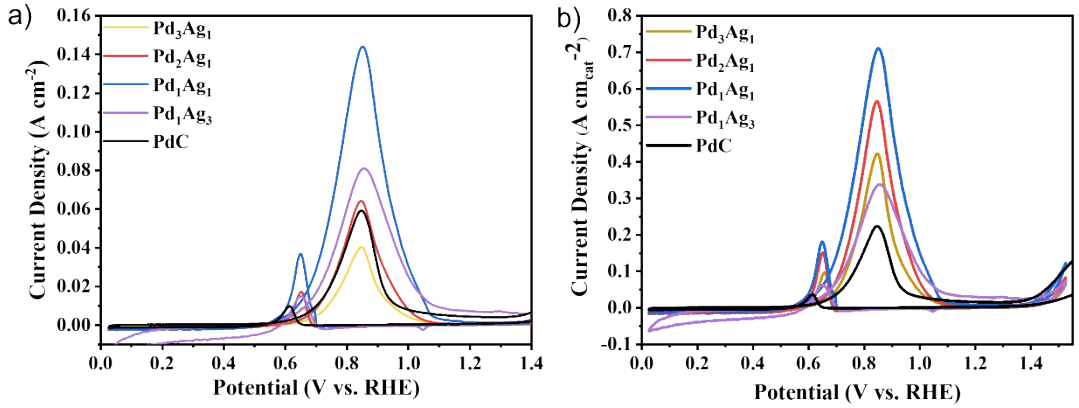

Fig. S3 CV curves of Pd_xAg_y NPs and Pd/C in 1 M KOH and 1 M EG solution normalized with (a) carbon glass area and (b) ECSA, respectively.

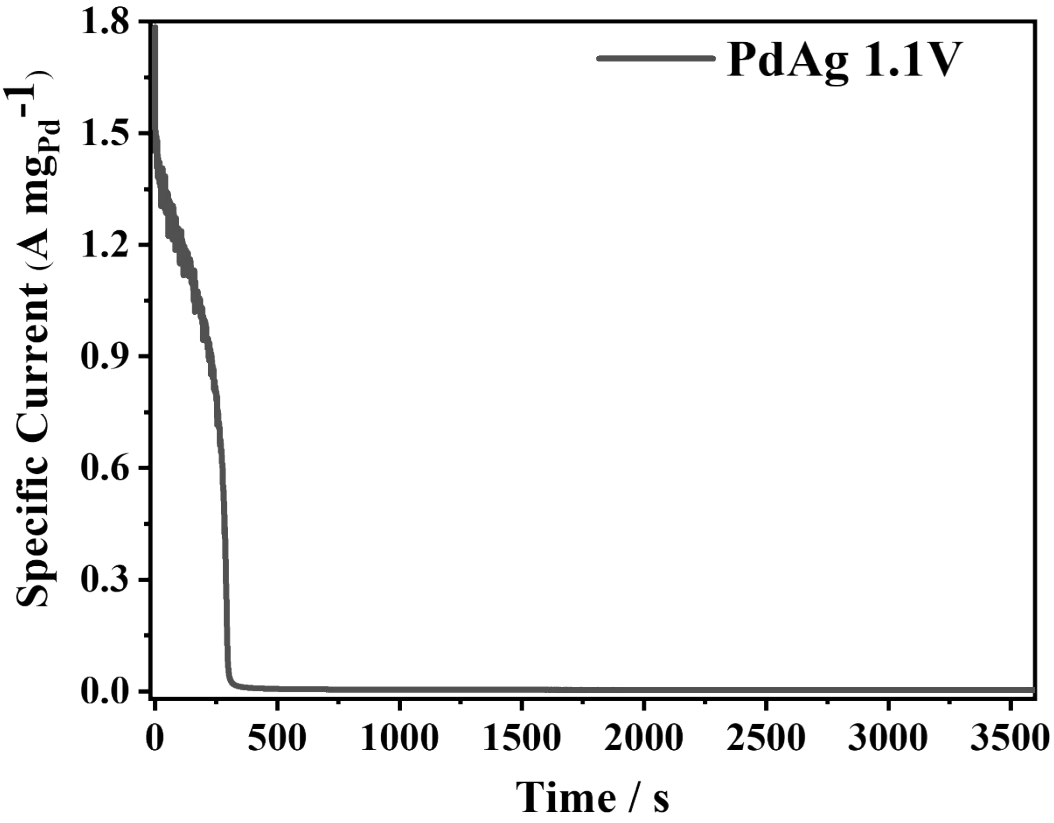

Fig. S4 i-t curves of Pd_1Ag_1 NPs at voltage of 1.1V vs. RHE for 1h.

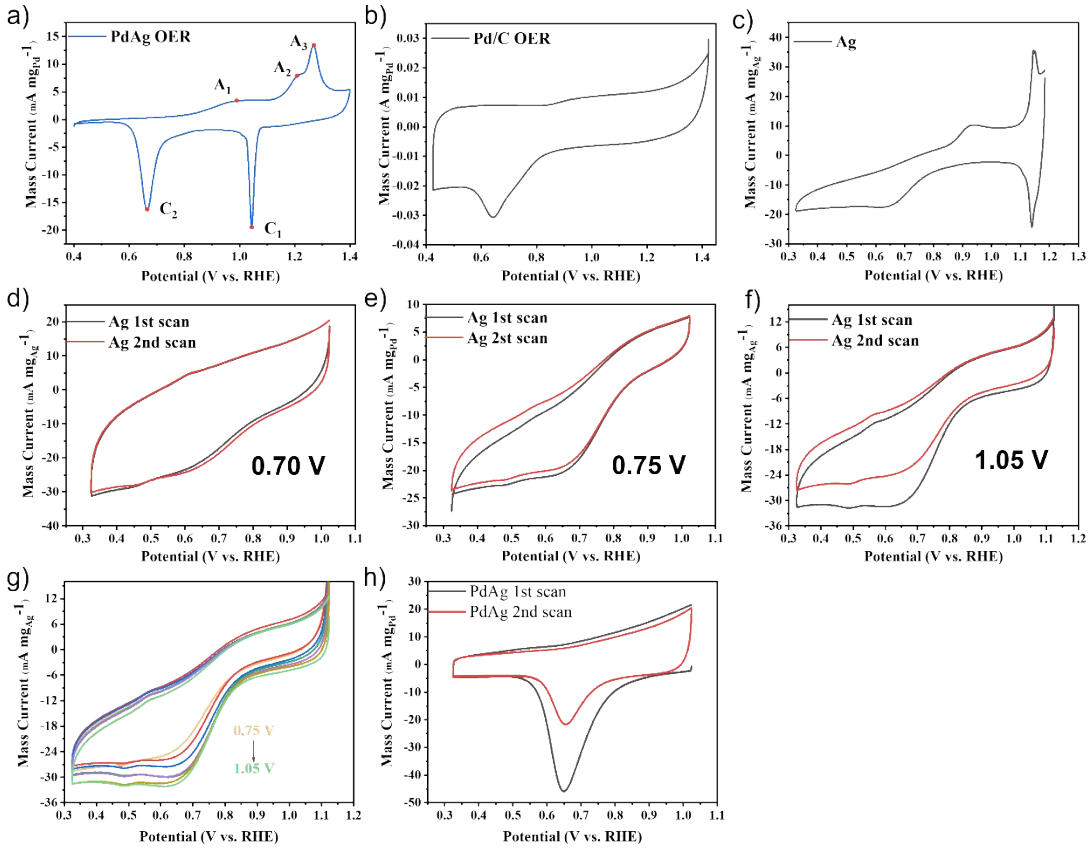

Fig. S5 CV curves of (a) Pd_1Ag_1 NPs, (b) Pd/C, and (c) Ag NPs in 1 M KOH solution. CV curves of Ag NPs after chronoamperometry at (d) 0.7 V, (e) 0.75 V, and (f) 1.05 V. (g) Comparison of the *OH desorption voltage range of Ag NPs after chronoamperometry at different voltages. (h) CV curves of Pd_1Ag_1 NPs after chronoamperometry at 1.05 V.

In order to verify the electrochemical behavior on the Pd_1Ag_1 NPs surface, cyclic voltammetry (CV) scans in 1 M KOH aqueous solution were performed (Figure S5a). Compared with CV scans on Pd/C and Ag NPs (Figure S5b and c), each anodic process, A_n, and its corresponding cathodic process, C_n, are defined. A_1 is associated with the oxidation of Pd and *OH adsorption processes. The formation of the AgOH-$Ag(OH)_2^-$ monolayer is associated with A_2. A_3 is attributed to the formation of Ag_2O multilayer.[1-4] Upon inversion of the scan direction toward negative potentials, two cathodic peaks appear. C_1 most likely corresponds to the formation of Ag^0. C_2 comes from the reduction of PdO and the desorption of *OH. To determine the potential range of the adsorption of *OH on the silver surface, CV scanning was performed immediately after chronoamperometry at different voltages. After applying a constant voltage of 0.7 V, the current of the first scan is slightly less than that of the second scan when scanning in the voltage range of 0.6-0.7 V, indicating that the voltage of 0.7 V is insufficient for *OH generation (Figure S4d). The weak *OH desorption current signal comes from the adsorption in the high voltage range during the cycle. On the second scan, more *OH is desorbed than on the first lap due to a longer holding time in the high voltage region. With the constant voltage increasing from 0.75V to 1.05V, the current signal of *OH desorption increases gradually (Figure S5e, f, and g). In the same way, the obvious *OH

desorption process can be observed on the Pd_1Ag_1 NPs (Figure S5h), indicating that Ag atoms can act as an additional *OH generation site to provide reactive oxygen species to assist in the rapid removal of toxic species from the Pd surface. However, on the Pd/C surface, the competition between EG and water adsorption limits the free sites to produce hydroxyl group species[5].

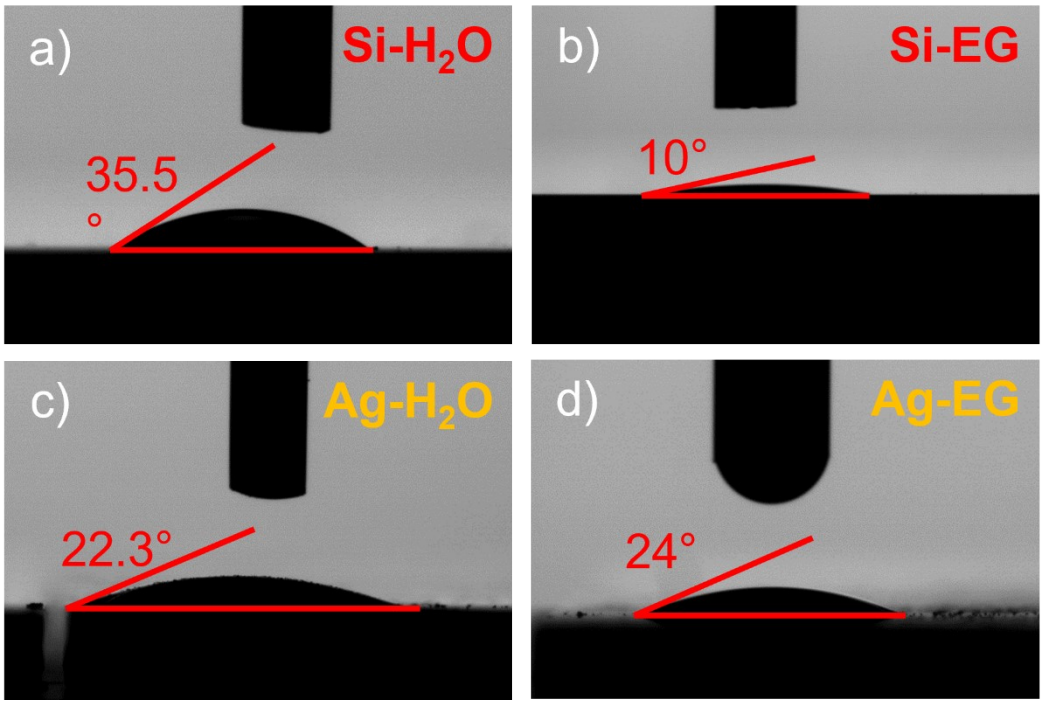

Fig. S6 (a) H_2O and (b) ethylene glycol contact angle on silicon wafer. (c) H_2O and (b) ethylene glycol contact angle on Ag nanoparticles spin-coated on silicon wafer.

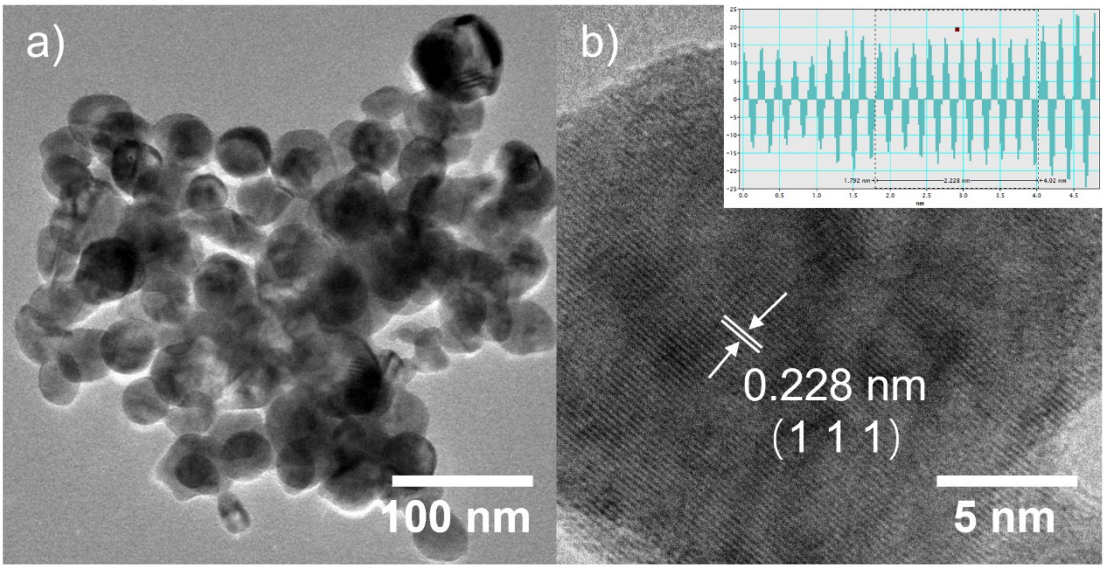

Fig. S7 The morphology of the samples after a long-term electro-reforming.

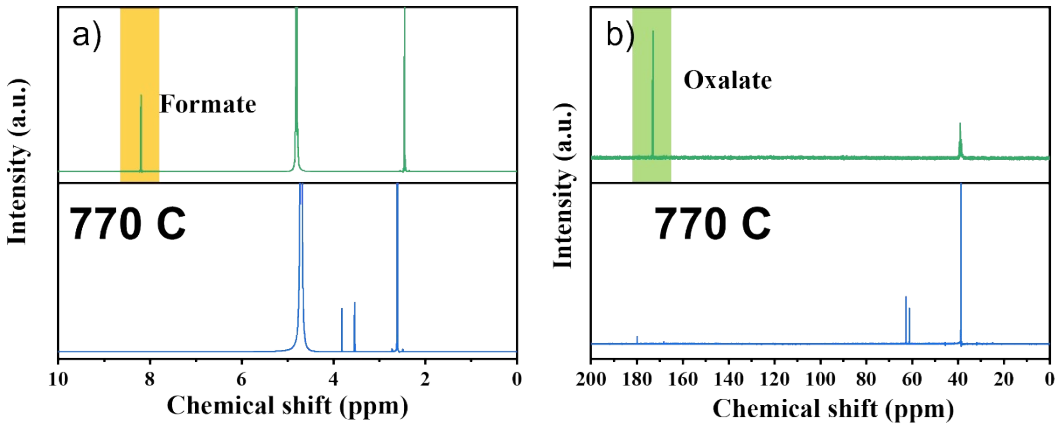

Fig S8 (a) ^{1}H NMR and (b) ^{13}C NMR spectra of the electrolyte and standard sample.

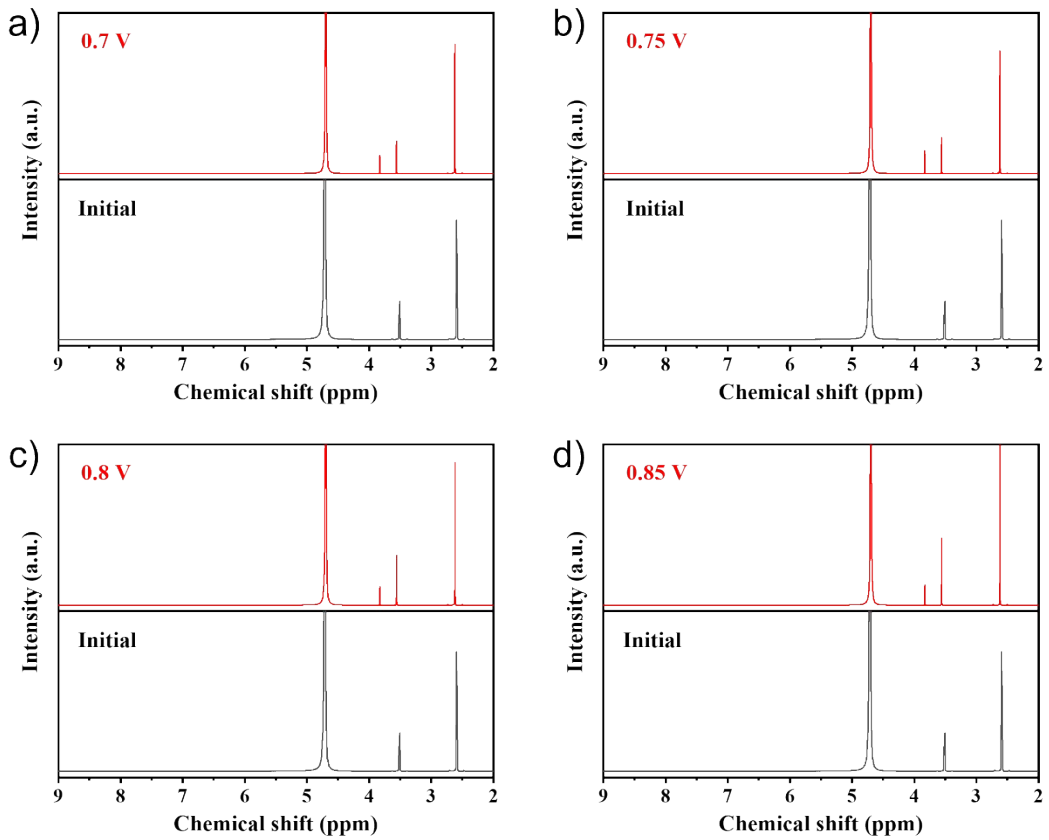

Fig. S9 ^{1}H spectra of the electrolyte with EG conversion of about 50% under different voltages.

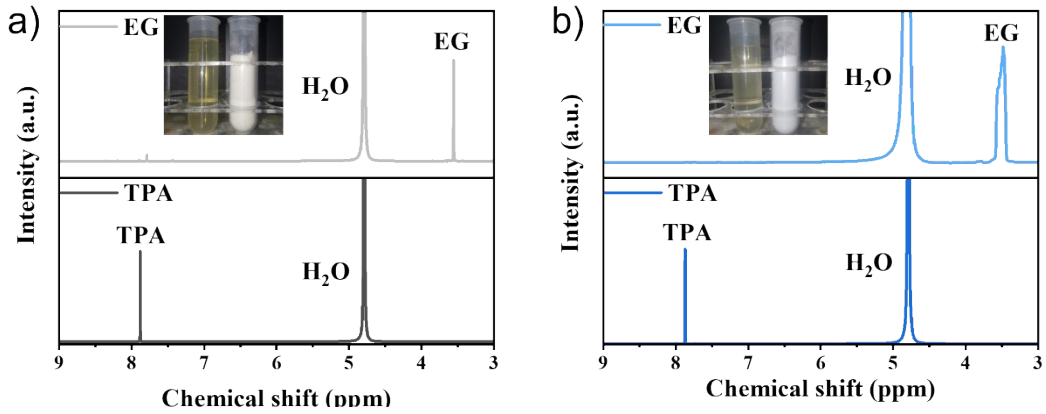

Fig. S10 ^{1}H spectra of hydrolysates from (a) transparent and (b) blue PET bottles.

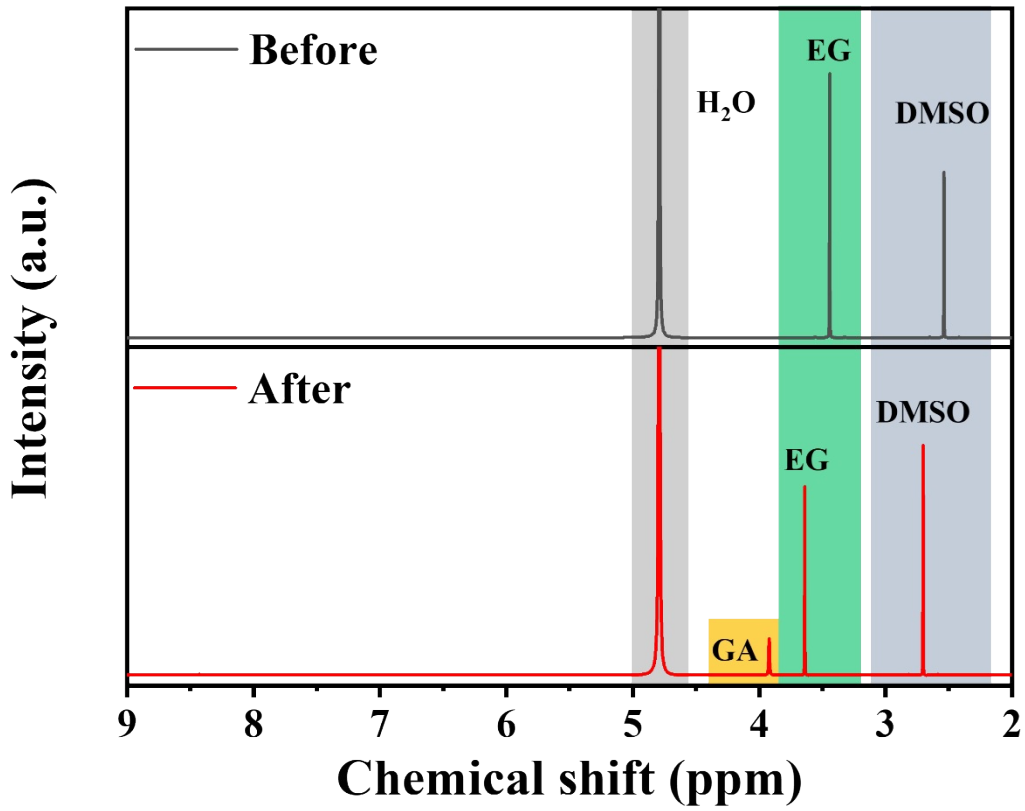

Fig. S11 Comparison of ^1H spectra of electrolyte before and after electro-reforming in a flow cell.

Table S1. Summary of ICP results and ECSA determined from CV curves for different Pd and alloy electrocatalysts under study.

	Pd wt%	**Ag wt%**	**ECSA (m^2 g^{-1})**
10 wt% PdC	10	-	10.01
Pd_3Ag_1	67.7	32.3	1.01311
Pd_2Ag_1	60	40	1.07242
Pd_1Ag_1	45.5	54.5	1.43523
Pd_1Ag_2	30.4	69.6	1.72166
Pd_1Ag_3	21.2	78.8	0.85037

Table S2. EGOR stability of PdAg NPs and various electrocatalysts from published works.

electrocatalyst	Electrolyte	Chronoamperometric stability	Reference
PdAg NPs	1.0 M KOH + 1.0 M EG	83% activity retention after 3600s	This work
PtPd alloyed multipods	1.0 M KOH + 1.0 M EG	1.7% activity retention after 3600s	[6]
PdAg/C	0.5 M KOH + 0.5 M EG	51% activity retention after 3000s	[7]
Pd-PdSe HNSs	1.0 M KOH + 1.0 M EG	47% activity retention after 3600s	[8]
AuPd@Pd	0.5 M KOH + 0.5 M EG	25.6% activity retention after 3600s	[9]
PdAu core-shell nanospheres	1.0 M KOH + 1.0 M EG	5% activity retention after 3600s	[10]
PdNi nanospheres	1.0 M KOH + 1.0 M EG	4.6% activity retention after 3600s	[11]
PdAu-NF/NG	1.0 M KOH + 1.0 M EG	15.5% activity retention after 3600s	[12]
PtPd ANPs/ 3D-N-rGO	0.5 M KOH + 0.5 M EG	18.8% activity retention after 3600s	[13]
Pd–Bi_2Te_3 /Pd	1.0 M KOH + 1.0 M EG	26% activity retention after 3600s	[14]

Table S3. Peak assignments for the infrared spectra of EGOR on Pd_1Ag_1 NPs and Pd/C in alkaline media acquired by two reflection modes.

Wavenumber/cm^{-1}	**Assignment**
1309	Feature peak for oxalate[15, 16]
1326	Symmetric stretch of COO^- in glycolate[15, 17]
1405	Symmetric stretch of COO^- in glycolate on PdC[16, 17]
1415	Symmetric stretch of COO^- in glycolate on Pd_1Ag_1 NPs[16, 17]
1580	Asymmetric stretch of COO^- in glycolate[15, 17]
1630	ν(C=O) of adsorbed 2-hydroxyacetyl[18, 19]
1835-1890	Adsorbed CO species[20, 21]

1. Sayed S. Abd El Rehim*, Hamdy H. Hassan, Magdy A. M. Ibrahim and M. A. Amin, *Monatsh. Chem.*, 1998, **129**, 1103–1117
2. T. P. Dirkse, *Electrochim. Acta*, 1990, **35**, 1445-1449.
3. J. Ambrose and R.G. Barradas, *Electrochim. Acta*, 1974, **19**, 781-786.
4. I. R. Zamora-Garcia, A. Alatorre-Ordaz, J. G. Ibanez, M. G. Garcia-Jimenez, Y. Nosaka, T. Kobayashi and S. Sugita, *Electrochim. Acta*, 2013, **111**, 268-274.
5. J. L. Lin, J. Ren, N. Tian, Z. Y. Zhou and S. G. Sun, *J. Electroanal. Chem.*, 2013, **688**, 165-171.
6. J. J. Lv, L. P. Mei, X. Weng, A. J. Wang, L. L. Chen, X. F. Liu and J. J. Feng, *Nanoscale*, 2015, **7**, 5699-5705.
7. Y. Yang, W. Wang, Y. Liu, F. Wang, Z. Zhang and Z. Lei, *Int. J. Hydrog. Energy*, 2015, **40**, 2225-2230.
8. Y. Qin, W. Zhang, F. Wang, J. Li, J. Ye, X. Sheng, C. Li, X. Liang, P. Liu, X. Wang, X. Zheng, Y. Ren, C. Xu and Z. Zhang, *Angew. Chem. Int. Ed.*, 2022, **61**, e202200899.
9. Q. Liu, Y.-R. Xu, A.-J. Wang and J.-J. Feng, *Int. J. Hydrog. Energy*, 2016, **41**, 2547-2553.
10. H. Xu, B. Yan, K. Zhang, J. Wang, S. Li, C. Wang, Y. Shiraishi, Y. Du and P. Yang, *J. Alloys Compd.*, 2017, **723**, 36-42.
11. K. Zhang, H. Xu, B. Yan, J. Wang, Y. K. Du and Q. Y. Liu, *Electrochim. Acta*, 2018, **268**, 383-391.
12. H. Xu, B. Yan, K. Zhang, J. Wang, S. Li, C. Wang, Y. Shiraishi, Y. Du and P. Yang, *Electrochim. Acta*, 2017, **245**, 227-236.
13. Y.-C. Shi, J.-J. Feng, X.-X. Lin, L. Zhang, J. Yuan, Q.-L. Zhang and A.-J. Wang, *Electrochim. Acta*, 2019, **293**, 504-513.
14. H. Xu, B. Huang, Y. Zhao, G. He and H. Chen, *Inorg. Chem.*, 2022, **61**, 4533-4540.
15. L. Wang, H. Meng, P. K. Shen, C. Bianchini, F. Vizza and Z. Wei, *Phys. Chem. Chem. Phys.*, 2011, **13**, 2667-2673.
16. H. Wang, B. Jiang, T.-T. Zhao, K. Jiang, Y.-Y. Yang, J. Zhang, Z. Xie and W.-B. Cai, *ACS Catal.*, 2017, **7**, 2033-2041.
17. P.A. Christensen and A. Hamnett, *J. Electroanal. Chem. Inter. Electrochem.*, 1989, **260**, 347-359.
18. J. Schnaidt, M. Heinen, Z. Jusys and R. J. Behm, *J. Phys. Chem. C*, 2012, **116**, 2872-2883.
19. J. Schnaidt, M. Heinen, Z. Jusys and R. J. Behm, *Catal. Today*, 2013, **202**, 154-162.
20. Y. Y. Yang, J. Ren, H. X. Zhang, Z. Y. Zhou, S. G. Sun and W. B. Cai, *Langmuir*, 2013, **29**, 1709-1716.
21. Y.-Y. Yang, J. Ren, Q.-X. Li, Z.-Y. Zhou, S.-G. Sun and W.-B. Cai, *ACS Catal.*, 2014, **4**, 798-803.